Wind Energ. Sci. Discuss., doi:10.5194/wes-2016-21, 2016
Manuscript under review for journal Wind Energ. Sci.
Published: 17 June 2016

eawe european academy of wind energy
Open Access WIND ENERGY SCIENCE DISCUSSIONS

Wind turbine power production and annual energy production depend on atmospheric stability and turbulence

Clara M. St. Martin,[1] Julie K. Lundquist,[1,2] Andrew Clifton,[2] Gregory S. Poulos,[3] and Scott J. Schreck[2]

[1] Department of Atmospheric and Oceanic Sciences (ATOC), University of Colorado at Boulder, 311 UCB, Boulder, CO, 80309

[2] National Renewable Energy Laboratory, 15013 Denver West Parkway, Golden, CO, 80401

[3] V-Bar, LLC, 1301 Arapahoe Street, Suite 105, Golden, CO, 80401

Correspondence to: Clara M. St. Martin (clara.st.martin@colorado.edu)

Wind Energ. Sci. Discuss., doi:10.5194/wes-2016-21, 2016
Manuscript under review for journal Wind Energ. Sci.
Published: 17 June 2016

Abstract. Using detailed upwind and nacelle-based measurements from a General Electric [GE] 1.5sle model with a 77m rotor diameter, we calculated power curves and annual energy production (AEP) and explored their sensitivity to different atmospheric parameters. This work provides guidelines for the use of stability and turbulence filters in segregating power curves to gain a clearer picture of the power performance of a turbine. The wind measurements upwind of the turbine include anemometers mounted on a 135m meteorological tower and lidar vertical profiles. We calculated power curves for different regimes based on turbulence parameters such as turbulence intensity (TI) and turbulence kinetic energy (TKE), as well as atmospheric stability parameters such as Bulk Richardson number (R_B). AEP was also calculated with and without these atmospheric filters and differences between these calculations are highlighted in this article. The power curves for different TI and TKE regimes revealed that, at the U.S. Department of Energy (DOE) National Wind Technology Center (NWTC) at the National Renewable Energy Laboratory (NREL), increased TI and TKE undermined power production at wind speeds near rated, but increased power production at lower wind speeds. Similarly, power curves for different R_B regimes revealed that periods of stable conditions produced more power at wind speeds near rated and periods of unstable conditions produced more power at lower wind speeds. AEP results suggest that calculations done without filtering for these atmospheric regimes may be overestimating the AEP. Because of statistically significant differences between power curves and AEP calculated with these turbulence and stability filters for this turbine at this site, we suggest implementing an additional step in analyzing power performance data to take atmospheric stability and turbulence across the rotor disk into account.

Keywords

wind energy, power curve, atmospheric stability, TI

1 Introduction

Calculating and understanding a wind turbine power curve is crucial for power performance testing and annual energy production (AEP) assessments. Previous work on power performance emphasizes the role of turbulence intensity (TI) and wind shear in influencing power production (Elliot and Cadogan, 1990; Hunter et al., 2001; Kaiser et al., 2003; Sumner and Masson, 2006; Gottschall and Peinke, 2008; Antoniou et al., 2009; Rareshide et al., 2009; Wharton and Lundquist, 2012a, 2012b; Clifton et al., 2013; Dörenkämper et al., 2014). Wharton and Lundquist

Wind Energ. Sci. Discuss., doi:10.5194/wes-2016-21, 2016
Manuscript under review for journal Wind Energ. Sci.
Published: 17 June 2016

(2012b) also found that vertical TI and turbulence kinetic energy (TKE) affect power performance and Rareshide et al. (2009) found that veer affects power performance. Previous work also shows that atmospheric stability induces deviations of power from the manufacturer power curve (MPC) (Motta et al., 2005; van den Berg, 2008; Vanderwende and Lundquist, 2012; Wharton and Lundquist, 2012b). Some work has also focused on atmospheric variations across the rotor disk that influence the power performance results (Sumner and Masson, 2009; Wagner et al., 2009; Choukulkar et al., 2015).

Because the power curve is so closely tied to AEP, factors that influence the power performance typically influence AEP calculations as well. The two most closely explored atmospheric factors with regard to AEP are TI and wind shear, but the existing studies do not agree on the influence of TI and wind shear on AEP. The simulation-based study of Antoniou et al. (2009) found that low wind shear supported high AEP. For low wind speeds, the highest AEP occurred during conditions of high TI, but at higher wind speeds, the highest AEP occurred when TI was low. In their analysis of data from a number of wind farms, Rareshide et al. (2009) also compared AEP calculated with different TI and shear combinations, and found that AEP typically decreased with increasing TI, but increased with increasing shear, in contrast to the findings of Antoniou et al. (2009).

In this study, we also investigated the influence of different atmospheric stability and turbulence regimes on wind turbine power curves and AEP calculations, incorporating a broad set of atmospheric parameters as well as different approaches to measuring these parameters. In Sect. 2 we describe our data set, which includes an upwind meteorological (met) tower with measurements spanning the rotor disk as well as wind-profiling lidar. In Sect. 3 we present our data analysis methods, which include filtering the data by atmospheric parameters like shear, TI, and atmospheric stability. The effects of atmospheric parameters on power curves and AEP are presented in Sect. 4, and in Sect. 5 we summarize conclusions about the effects of atmospheric stability and inflow turbulence on power curves and AEP calculations.

2 Data

2.1 Measurement site

The measurements used in this analysis were collected at the U.S. Department of Energy (DOE) National Wind Technology Center (NWTC, Fig. 1) at the National Renewable Energy Laboratory (NREL), located just south of

Wind Energ. Sci. Discuss., doi:10.5194/wes-2016-21, 2016
Manuscript under review for journal Wind Energ. Sci.
Published: 17 June 2016

Boulder, Colo., and about 5 km east of the Colorado Front Range (Clifton et al., 2013; Aitken et al., 2014). The prevailing wind direction at 80 m (hub height) at this site during this campaign (29 November 2012 – 14 February 2013) was west–northwesterly.

This wind direction also dominated a 14-year period from a neighboring met tower at the NWTC (Clifton and Lundquist, 2012). During the winter, the downslope flow from the nearby Rocky Mountains is frequently channeled through Eldorado Canyon, located just west–northwest of the NWTC (Banta et al., 1996; Poulos et al., 2000, 2007; Clifton et al. 2013; Aitken et al., 2014). The NWTC site slopes upward about 20 m in elevation change toward the west. The surface is mostly short grass.

2.2 Upwind measurements

Upwind measurements were taken using a Renewable NRG Systems (NRG)/LEOSPHERE WINDCUBE v1 vertically profiling Doppler lidar (Courtney et al., 2008; Rhodes and Lundquist, 2013) and a 135m met tower. The tower includes several levels of cup anemometers, vanes, sonic anemometers, and temperature sensors, along with precipitation and air-pressure sensors (Fig. 2, Table 1), all on booms pointing in the dominant wind direction (west–northwest). Data were collected during the winter at times of strongest winds at the NWTC (from 29 November 2012 through 14 February 2013). The lidar is located about 215 m (2.8D) west of the General Electric (GE) 1.5sle turbine on the NWTC site. The met tower is located about 170 m (2.2D) west–northwest of the turbine (Fig. 1). Because different instruments employ different averaging methods, Fig. 3 shows that all wind speed data sets were synchronized and illustrates how the power output responds.

2.2.1 Lidar

The NRG/LEOSPHERE WINDCUBE v1 lidar measures volumetric-averaged wind speeds and directions every 20 m from 40 m to 220 m, thereby spanning the entire vertical extent of the turbine rotor disk. The wind speeds are measured with an accuracy of 0.2 m s^{-1} and the wind directions are measured at an accuracy of 1.5° (Pauliac, 2009). First, we filtered the nominally 1Hz measurements of the horizontal wind speeds and directions for suitable carrier-to-noise ratio (CNR). Next, we averaged to 10 min for comparison with the tower and turbine data. The lidar takes a volumetric measurement, assuming homogeneity over the entire volume it is measuring. This process introduces an

Wind Energ. Sci. Discuss., doi:10.5194/wes-2016-21, 2016
Manuscript under review for journal Wind Energ. Sci.
Published: 17 June 2016

uncertainty in the lidar measurements in inhomogeneous flow (Bingöl et al., 2009; Rhodes and Lundquist, 2013; Lundquist et al., 2015); this possible source of error is discussed in further detail in the supplement (Sect. S1).

2.2.2 Meteorological tower

The M5 met tower (NWTC, 2016, similar to the M4 tower at the site, which was studied by Rinker et al., 2016) is instrumented with cup anemometers at 3, 10, 30, 38, 55, 80, 87, 105, 122, and 130 m, and vanes at 3, 10, 38, 87, and 122 m (Fig. 2 and Table 1). Barometric pressure and precipitation sensors are located at 3 m and temperature sensors at 3, 38, and 87 m (Table 1). Sonic anemometers are mounted at 15, 41, 61, 74, 100, and 119 m (Fig. 2 and Table 1). The tower booms are directed at 278°, into the prevailing wind direction, slightly north of west. Measurements from the sonic anemometers at 15 m were used to calculate turbulent fluxes of momentum and heat for assessment of atmospheric stability as discussed in the following sections.

2.3 Wind turbine data

A GE 1.5MW turbine (GE 1.5/77 sle) with an 80m hub height was chosen for this study. The GE 1.5MW is the most widely deployed utility-scale turbine in the world with more than 12,000 turbines deployed around the globe as of 2009 (GE Energy, 2009). The supervisory control and data acquisition (SCADA) system of the DOE GE 1.5sle turbine provides 10min averages of nacelle wind speed, nacelle orientation, turbine power, and blade pitch angles. These measurements can be compared with the upwind measurements to quantify power curves and AEP. The cup anemometer mounted on the nacelle of the turbine is a NRG IceFree Hybrid XT Turbine Control Anemometer. The GE 1.5sle reaches its nameplate capacity, 1.5 MW, at a wind speed of 14 m s^{-1} (GE Energy, 2009). We refer to this wind speed as the rated wind speed for the rest of this article. The lower and upper extremes of the swept area of the GE 1.5sle in this study were 41.5 m and 118.5 m above ground. More details on this turbine and power performance testing results as well as instrument and site calibration information can be found in Mendoza et al. (2015).

3 Analysis methods

Before calculating atmospheric parameters, all meteorological and turbine data were checked for data quality as described in Sect. 3.1.

3.1 Data quality control

Wind Energ. Sci. Discuss., doi:10.5194/wes-2016-21, 2016
Manuscript under review for journal Wind Energ. Sci.
Published: 17 June 2016

eawe european academy of wind energy
Open Access WIND ENERGY SCIENCE DISCUSSIONS

3.1.1 Lidar

All lidar-measured wind-speed measurements were filtered by CNR: only measurements with a CNR greater than –18 dB were retained. Lower CNR results from clean-air conditions (Aitken et al., 2012), which occur frequently on Colorado's Front Range in the winter. After additional filtering for quality control purposes (such as removing bad data as defined by the manufacturer's wind speed and temperature limits), the data recovery rate was approximately 33.5 % for horizontal wind speeds and directions at 40 m, 40 % for horizontal wind speeds and directions at 60 and 120 m, and 45 % for horizontal wind speeds and directions at 80 and 100 m.

3.1.2 Meteorological tower

Quality control filtering methods performed on the met tower data followed procedures including discarding data that were flagged because of irregular timing (when the time between measurements was inconsistent), insufficient number of data points within a 10min averaging period according to the manufacturer, low standard deviation (less than 0.01 % of the mean) or constant values during the measurement interval (which indicate icing events), empty data channels, bad values as defined by manufacturer limits, or when an instrument recorded a "NaN" in place of a real measurement. After filtering for quality control purposes, the met tower measured horizontal wind speeds and directions and temperatures about 90 % of the time at all levels during this study.

3.2 Wind speed and direction subselection

Although the dominant wind direction at the site is west–northwesterly, other wind directions do occur. To ensure the lidar and met tower measurements were wake-free (upwind of the turbine), we considered only data from time periods of hub height wind from the 235°–315° wind direction sector. This sector includes the most frequent and highest wind speeds as measured by both upwind instruments (Fig. 4). Only wind speeds between cut-in (3.5 m s^{-1}) and cut-out (25 m s^{-1}) were considered to ensure that the turbine was operating.

3.3 Filtering turbine underperformance

After filtering for quality control as well as wind speed and direction, we still saw a large number of times when the turbine was producing significantly less power than expected—underperforming— relative to most of the points, as

Wind Energ. Sci. Discuss., doi:10.5194/wes-2016-21, 2016
Manuscript under review for journal Wind Energ. Sci.
Published: 17 June 2016

seen in Fig. 5a. However, blade pitch angles can be used to segregate data and flag most of these underperforming periods, as follows.

Without access to the turbine control system or data more refined than 10min averages, typical blade pitch angles can be quantified as a function of wind speed (Fig. 5b). The median value for blade pitch angle for each wind speed bin as well as $\pm$ 3 median absolute deviation (MAD) are shown by the red envelope in Fig. 5b. We used MAD here instead of mean absolute deviation so that a few outliers would not bias the calculation. When plotted on a power curve using the tower 80m cup anemometer for wind speed, Fig. 5a, the majority of the points outside of the $\pm$ 3 MAD and between 5 and 17 m s^{-1} showed underperformance. To filter for underperformance, then, we calculated MAD blade pitch angles from each blade for each wind speed bin between 5 and 17 m s^{-1}. Time periods with blade pitch angle outside of $\pm$ 3 MAD were discarded. Although it is possible that variability on timescales shorter than 10 min may affect turbine operation, the effective filtering seen in the magenta scatter in Fig. 5a suggests that this approach is sufficient. This filtering by blade pitch angle also has the advantage of using only data to which a typical wind plant operator would have access.

After filtering for hub height wind speed and direction, positive power production, and blade pitch angle, 1,214 out of 7,949 lidar 80m wind speed data points remained (15 %), and 2,196 out of 9,918 met tower 80m wind speed data points remained (20 %). Concurrent lidar, met tower, and turbine data that fulfilled the various screening criteria occurred during 1,083 10min periods.

3.4 Power curves

Power curves based on wind speeds normalized by air density following International Electrotechnical Commission (IEC) 61400-12-1 (2015) can be used to evaluate turbine performance. The observed power curves, comparing power production to 80m tower anemometer wind speeds (Fig. 6a), 80m lidar wind speeds (Fig. 6b), and nacelle anemometer wind speeds (Fig. 6c), generally showed good agreement with an approximation of the MPC (GE Energy 2009). This approximated MPC was determined by placing the publically available MPC for the GE 1.5sle on a grid (with dimensions of 0.5 m s^{-1} by 50 kW) and estimating expected power produced at each wind bin.

The power curves created from 10min tower and nacelle-mounted anemometers (Fig. 6a, Fig. 6c, respectively) showed less variability than the lidar power curve (Fig. 6b). It is especially apparent from the power

Wind Energ. Sci. Discuss., doi:10.5194/wes-2016-21, 2016
Manuscript under review for journal Wind Energ. Sci.
Published: 17 June 2016

curve created from 10min lidar measurements (Fig. 6b) that the lidar variability at this particular site is vulnerable to inhomogeneity in the flow. Although lidars are widely available and used in the field (Clifton 2015), the variability between the lidar and tower measurements (Fig. 7) indicated sufficient inhomogeneity in the flow at this particular site (as observed by Aitken et al., 2014) to cause us to discuss and show only the upwind data from the tower from this point forward. Note, however, that not all sites are subject to the inhomogeneity seen at the NWTC, and all instruments available for wind measurement should be considered. Concurrent met tower and turbine data that fulfilled the screening criteria occurred during 2,186 10min periods, equivalent to about 364 h of data, which is more than twice the 180 h of data that the IEC 61400-12-1 standard (2015) recommends for power performance testing.

3.5 Atmospheric stability regimes

Numerous approaches are available for classifying the atmospheric stability of a given 10min time period. Bulk Richardson number (R_B) calculations use temperature and wind speed differences from the lowest met tower measurement to the height of the top of the rotor disk to compare the buoyant production of turbulence to the wind-shear-generated mechanical production of turbulence (Stull, 1988) as

$$R_B = \frac{g\,\Delta T\,\Delta z}{\bar{T}\,\Delta U^2}\ , \tag{1}$$

where g is the gravitational constant, Δz is the change in height, ΔT is the change in 10min averages of temperature across Δz, $\bar{T}$ is the mean temperature across Δz, and ΔU is the change in the 10min averages of horizontal wind speed across Δz. Note that Eq. (1) does not consider wind direction variability because cup anemometer measurements provide only information about horizontal wind speed. Typical stability classifications based on R_B calculations are as follows: turbulent flow in unstable conditions when R_B is less than 0, laminar flow in stable conditions when R_B is greater than 0.25, and neutral conditions when R_B is between 0 and 0.25 (Stull, 1988). These stability classifications are similar to those used in previous work on stability effects on wind turbine fatigue and loading in Kelley (2011), and slightly different from the stability classifications used in Vanderwende and Lundquist (2012). The distribution of R_B calculated from the tower measurements for this campaign (Fig. 8), however, suggested that slightly different regimes, shown in Table 2, could be used to better represent the data at this site. R_B regimes are similarly defined for the NWTC in Aitken et al. (2014).

Wind Energ. Sci. Discuss., doi:10.5194/wes-2016-21, 2016
Manuscript under review for journal Wind Energ. Sci.
Published: 17 June 2016

Obukhov length *(L)* is also a useful measure of atmospheric stability, relying on surface stresses as well as heat fluxes to estimate the height in the surface layer at which the buoyant production of turbulence dominates wind-shear-generated mechanical production of turbulence (Stull, 1988) as

$$L = -\frac{u_*^3}{k\,g}\frac{T_v}{\overline{w'T_s'}} \quad , \tag{2}$$

where u_* is the friction velocity, k is the von Karman constant 0.4, T_v is the virtual temperature, w' is the vertical wind speed fluctuation in the 10min averaging period, and T_s' is the sonic temperature fluctuation in the 10m averaging period. Typical stability classifications are used in this work and are based on L calculations as defined by Muñoz-Esparza et al. (2012); shown in Table 2. These classifications are slightly different from those used in Wharton and Lundquist (2012b). The distributions of L are shown in Fig. 9.

When the R_B and L stability approaches are compared against one another and against time-of-day, as in Fig. 10, the different stability parameters differ slightly in their definitions of unstable and stable. Because of differences in stability classes using these different stability parameters, along with their different approaches to defining atmospheric stability, we treated R_B-defined stability classes separately from L-defined stability classes in the power curves.

3.6 Turbulence regimes

TI can also be used to describe atmospheric conditions, as demonstrated by Rareshide et al. (2009), Wagenaar and Eecen (2011), and Wharton and Lundquist (2012a). TI is typically defined as

$$TI = \frac{\sigma_{80m}}{U_{80m}} * 100 \quad , \tag{3}$$

where σ_{80m} is the 10min standard deviation of the horizontal wind speed at 80 m and U_{80m} is the 10min mean horizontal wind speed at 80 m. Although the TI approach has been used successfully at other locations, the NWTC consistently features strong turbulence likely resulting from the terrain characteristics of the site (Fig. 11, Fig. 12), making it difficult to distinguish typical stability classes from TI calculations. This strong ambient turbulence has led to the choice of site-specific turbulence classification defined in Table 3.

Wind Energ. Sci. Discuss., doi:10.5194/wes-2016-21, 2016
Manuscript under review for journal Wind Energ. Sci.
Published: 17 June 2016

eawe european academy of wind energy
Open Access WIND ENERGY SCIENCE DISCUSSIONS

When the atmospheric stability regimes are compared to the TI regimes defined here (Fig. 13), the R_B and TI regime percentages also differ slightly in their definitions of unstable atmospheric conditions and highly turbulent conditions. Most of the daytime points are within the unstable regime as defined by R_B; however, only about 16 % of the data fall within unstable conditions with higher TI. This comparison, again, emphasizes the highly turbulent characteristics of the NWTC.

To further understand the turbulence characteristics demonstrated during this campaign, we also calculated TKE using the 74m 3D sonic anemometer mounted on the M5 met tower. Although TI is a parameter typically calculated and analyzed in the wind industry, TKE has the advantage of including the vertical component of the wind:

$$TKE = \frac{1}{2}\left(\overline{u'^2} + \overline{v'^2} + \overline{w'^2}\right) , \quad (4)$$

where we calculate TKE per unit mass, *u'* is the perturbation from a 10min average of the u-component of the wind, *v'* is the perturbation from a 10m average of the v-component of the wind, and *w'* is the perturbation from a 10min average of the w-component of the wind. Using this TKE approach also revealed the strong turbulence at the NWTC with little or no diurnal cycle (Fig. 11, Fig. 14). Turbulence classifications based on TKE were determined by the distribution in Fig. 14 and are listed in Table 3.

Many cases with relatively high TI or TKE are considered neutral and stable according to our stability definitions in Table 3. Depending on whether TI, TKE, R_B, or L is considered a measure of atmospheric stability, a particular time period may be classified differently. In other words, different results are found depending on the metric selected.

3.7 Wind shear regimes

To estimate the effect of the wind speed vertical profile across the rotor disk, the wind shear exponent or power law exponent parameter, α, is typically used in the wind energy industry:

$$\alpha = \frac{\log\left(\frac{U_2}{U_1}\right)}{\log\left(\frac{z_2}{z_1}\right)} , \quad (5)$$

Wind Energ. Sci. Discuss., doi:10.5194/wes-2016-21, 2016
Manuscript under review for journal Wind Energ. Sci.
Published: 17 June 2016

where z_1 is the reference height, z_2 is the height above ground level, U_2 is the wind speed at height z_2, and $U_1$is the wind speed at height z_1. At the NWTC during this study, the average wind shear exponent using the 122 m and 38 m tower wind speeds as z_2 and z_1 is 0.15. The standard deviation is 0.14 and the maximum wind shear exponent is 1.10, however. Although we found no statistically significant impact of wind shear on the power curves at this site, we did include shear exponent in the subsequent analysis, separating regimes of shear exponent as defined in Table 2 and based on the distribution in Fig. 15.

4 Results

To explore the variability in the power curves, we applied filters to the power curves based on factors such as atmospheric stability, TI, and TKE. We applied a new method to calculate AEP using these classifications. We can consider periods with low TI or TKE to be approximately "stable" by R_B and L; "unstable" conditions would generally have high TI and TKE. Our results showed that, generally, at this site with little veer, stable conditions (with varying degrees of significance) lead to overperformance at wind speeds just below rated power. Unstable conditions lead to overperformance at lower wind speeds with a few exceptions.

4.1 Power curves

The NWTC site generally exhibited high TI throughout this data collection period. Even so, some differences in power produced emerged at wind speeds between 5 and 7 m s^{-1} and at wind speeds between 10 and 14 m s^{-1} after separating the TI into relative classes of low, medium, and high TI (Fig. 16a, Fig. 16d, Fig. 17a, Fig. 17d, Table 3). Statistically distinct differences within each wind speed bin between the TI classes defined in Table 3 were determined by the Wilcoxon rank sum test with a 1 % significance level. These are denoted by closed circles in Fig. 16a, Fig. 16d, Fig. 17a, and Fig. 17d. This statistical test shows that for the power curves using nacelle winds, periods of relatively high TI produce significantly more power than periods of relatively low TI at wind speeds between 5 and 9 m s^{-1} (Fig. 16a, Fig. 17a). For the power curves using upwind tower winds, periods of relatively high TI produce significantly more power than periods of relatively low TI at wind speeds between 5 and 6.5 m s^{-1} (Fig. 16d, Fig. 17d). Conversely, power curves using nacelle winds show that at wind speeds between 10.5 and 13.5 m s^{-1}, periods of relatively low TI produce significantly more power than periods of relatively high TI. Power curves

Wind Energ. Sci. Discuss., doi:10.5194/wes-2016-21, 2016
Manuscript under review for journal Wind Energ. Sci.
Published: 17 June 2016

using upwind tower winds show that at wind speeds between 9.5 and 15.5 m s^{-1}, periods of relatively low TI produce significantly more power than periods of relatively high TI. Rareshide et al. (2009) found similar behavior.

On the other hand, power curves separated by R_B-defined stability class show only a few bins that are statistically distinct in power produced (Fig. 16b, Fig. 16e, Fig. 17b, Fig. 17e). Power curves using nacelle winds show that at some wind speeds between 5.5 and 9.0 m s^{-1}, periods of unstable conditions produce significantly more power than periods of stable conditions. Power curves using upwind tower winds show that at wind speeds around 7 m s^{-1}, periods of unstable conditions produce significantly more power than periods of stable conditions. Power curves using both nacelle winds and tower winds show that at wind speeds around 12 m s^{-1}, periods of stable conditions produce significantly more power than periods of unstable conditions.

Similarly, Fig. 16c, Fig. 16f, Fig. 17c, and Fig. 17f show periods of low TKE producing significantly more power at wind speeds just before rated than periods of high TKE, similar to the TI and R_B methods. Between 7.5 and 9.5 m s^{-1}, power curves using nacelle winds show that periods of high TKE produce significantly more power than periods of low TKE. Interestingly, however, power curves using upwind tower winds show that at 4 m s^{-1}, just after cut-in, periods of low TKE produce more power than periods of high TKE.

Distinct differences between power curves calculated from nacelle winds and power curves calculated from upwind tower winds occurred in the power curves of all three of these atmospheric parameters. Statistically distinct wind speed bins in power curves calculated from nacelle winds tended to be similar to those in power curves calculated from tower winds near rated speed. At lower wind speeds, however, between about 5 and 9 m s^{-1}, many more statistically distinct differences emerged between nacelle power curves than between tower power curves, most notably in the power curves segregated by TI regimes. Turbine operations were especially variable in this region of rapid increase in power with wind speed. The turbine reacted directly to the conditions as measured by instruments on the turbine.

Agreement between the TI, R_B, and TKE methods means that at wind speeds around rated, low TI, high stability, and low TKE result in overperformance relative to high TI, low stability, and high TKE. All three methods also agree that somewhere in between cut-in and rated, sometimes called “region 2,” high TI, low stability, and high TKE result in overperformance relative to low TI, high stability, and low TKE. Power curves separated by *L*-defined

Wind Energ. Sci. Discuss., doi:10.5194/wes-2016-21, 2016
Manuscript under review for journal Wind Energ. Sci.
Published: 17 June 2016

275 stability class do not show any statistically significant differences in power produced between unstable and stable periods (not shown).

4.2 Annual energy production

AEP allows developers and operators to quantify the projected energy production of a turbine. To quantify the impact on AEP of these stability- and turbulence-driven differences in power curves, we used a Weibull distribution
280 for wind speed and calculated AEP with no filter, as well as with TI, shear, and stability filters. These turbulence and stability filters for the AEP calculations can be further explained as AEP calculated using the power curves calculated from upwind tower winds shown in Fig. 16. These power curves are used together with a sample wind distribution using Weibull distribution parameters representative of the data set (λ = 10.13 m s^{-1}, k = 2.62) as suggested by IEC 61400 12-1 (2015) for a site-specific AEP. For each of these filters, separate AEP calculations
285 were made for each regime, weighted by the number of data points in that regime, and then added together to compare with the AEP calculated with no atmospheric filter. Note that although data were collected only during 2.5 months in the winter of 2012, AEP was calculated for an entire year to show values closer to a representative AEP value.

Results in Table 4 show a higher AEP when using no filter, followed by an AEP calculated with a TI filter
290 and then a shear filter. Although it is shown in the power curves in Fig. 16 and Fig. 17, a TKE filter to calculate AEP is not presented here because the result was a significantly smaller AEP, most likely resulting from the lack of data points in comparison to the other filters. The lower AEP calculated when separating by stability and turbulence regimes suggests that the AEP calculated using no filters may be overestimating the production, perhaps because the higher and lower extremes of the parameter ranges bias the averages in each bin.

295 When the AEP's low and high regimes are compared to the medium regimes of their respective atmospheric parameter, the AEP for medium-TI periods is higher than that for low-TI periods and for high-TI periods (Table 5). Using low- and high-TI power curves results in an AEP smaller than that calculated using the medium-TI power curve. These results are likely obtained because the low-TI power curve loses production at lower wind speeds and the high-TI power curve loses production around rated speed. When using a shear filter, the AEP
300 calculated with the high-shear power curve is higher than that with the low-shear power curve (Table 5).

Wind Energ. Sci. Discuss., doi:10.5194/wes-2016-21, 2016
Manuscript under review for journal Wind Energ. Sci.
Published: 17 June 2016

eawe european academy of wind energy
Open Access WIND ENERGY SCIENCE DISCUSSIONS

Conversely, when using a stability filter, the AEP calculated with the low-R_B power curve is higher than that with the high-R_B power curve (Table 5). This contrast between AEP calculated for the low stability regime and AEP calculated for the high stability regimes suggests that the unstable power curve (Fig. 16b,e) gains enough production near rated wind speed to surpass the production gain by the stable power curve (Fig. 16b,e) at lower wind speeds.

5 Conclusions

Using 2.5 months of data from upwind and nacelle-based instruments, we calculated power curves for different regimes of atmospheric stability and turbulence as well as AEP with and without these atmospheric filters. This work focuses not only on the idea of calculating different power curves for different atmospheric conditions for power performance testing, but also highlights the differences in AEP that can emerge from the application for stability- or turbulence-dependent power curves.

Statistically significant differences emerge among power curves segregated by TI, TKE, and R_B. At wind speeds between 5 and 7 m s^{-1}, during periods of high TI, significantly more power is produced than during periods of low TI. From about 10 to 14 m s^{-1} (near rated wind speed), during periods of low TI, significantly more power is produced than during periods of high TI. Similarly, periods of high TKE produce significantly more power between 7.5 and 9.5 m s^{-1} than during periods of low TKE, and periods of low TKE produce significantly more power around 12 m s^{-1} than during periods of high TKE. During periods of stable conditions, significantly more power is produced than during periods of unstable conditions around 12 m s^{-1}; significantly less power is produced than during periods of unstable conditions at some wind speeds between 5.5 and 8.5 m s^{-1}. Statistically significant distinctions in power curves did not occur when filtering for L, yaw error, wind shear, or wind veer for this data set at this site, perhaps explaining why stable conditions promote overperformance here, as in Wharton and Lundquist (2012b). A site with veer, however, exhibits underperformance in stable conditions (Vanderwende and Lundquist 2012).

After calculating an AEP for each regime and comparing the high and low regimes with the medium regime, differences between AEP calculated using different atmospheric filters are revealed. An AEP calculated with no atmospheric or turbulence filter is higher than any AEP calculated with these filters. In addition, the AEP calculated using a TI filter shows that the AEP calculated with the medium TI regime is greater than the AEP calculated with the low or high TI regimes. The AEP calculated with the shear filter shows that the high regime AEP

is higher than the AEP in the low and medium regimes; the AEP calculated with the R_B filter shows that the low regime AEP is much larger than the AEP in the high and medium regimes.

As discussed by Rareshide et al. (2009), manufacturers are increasingly filtering out data that represent what they consider anomalous or extreme atmospheric conditions for power performance testing. The IEC-61400-12-1 standard (2015) calls for at least 180 h of data to be used in a power performance test. Consequently, if manufacturers filter out data based on higher TI values, for instance, this means that more data must be gathered to make up for the discarded data. We see this discarding of data as unnecessary and potentially more costly. We suggest that instead of discarding these data, different power curves be calculated for different conditions. This will allow for a more refined understanding of how the turbine is operating in different atmospheric conditions, and may lead to a more accurate and reliable performance result and AEP calculation.

Acknowledgements

The authors express appreciation to the Center for Research and Education in Wind for supporting this work, to Thomas Fischetti at GE Power & Water for his assistance in turbine data collection and interpretation, and to the reviewers of a previous version of this work. This work was supported by the U.S. Department of Energy under Contract No. DE-AC36-08GO28308 with the National Renewable Energy Laboratory. Funding for the work was provided by the DOE Office of Energy Efficiency and Renewable Energy, Wind and Water Power Technologies Office.

The U.S. Government retains and the publisher, by accepting the article for publication, acknowledges that the U.S. Government retains a nonexclusive, paid-up, irrevocable, worldwide license to publish or reproduce the published form of this work, or allow others to do so, for U.S. Government purposes.

References

Aitken, M.L., Lundquist, J.K., Pichugina, Y.L., and Banta, R.M.: Quantifying wind turbine wake characteristics from scanning remote sensor data, J. Atmos. Ocean. Tech., 31, 765–787, doi:10.1175/JTECH-D-13-00104.1, 2014.

Aitken, M.L., Rhodes, M.E., and Lundquist, J.K.: Performance of a wind-profiling lidar in the region of wind turbine rotor disks, J. Atmos. Ocean. Tech., 29, 347–355, doi:10.1175/JTECH-D-11-00033.1, 2012.

Antoniou, I., Pedersen, S.M., and Enevoldsen, P.B.: Wind shear and uncertainties in power curve measurement and wind resources, Wind Engineering, 33, 449–468, doi:10.1260/030952409790291208, 2009.

Banta, R.M., Oliver, L.D., Gudiksen, P.H., and Lange, R.: Implications of small-scale flow features to modeling dispersion over complex terrain, J. Appl. Meteorol. , 35, 330–342, 1996.

Bingöl, F., Mann, J., and Foussekis, D.: Conically scanning LIDAR error in complex terrain, Meteorologische Zeitschrift, 18, 189–195, doi:10.1127/0941-2948/2009/0368, 2009.

Choukulkar, A., Pichugina, Y., Clack, C.T.M., Calhoun, R., Banta, R., Brewer, A. and Hardesty, M.: A new formulation for rotor equivalent wind speed for wind resource assessment and wind power forecasting, Wind Energy, doi: 10.1002/we.1929, 2015.

Clifton, A. Remote sensing of complex flows by Doppler wind lidar: issues and preliminary recommendations, NREL, Golden, Colo., 1–42, 2015.

Clifton, A., Kilcher, L., Lundquist, J. K., Fleming, P.: Using machine learning to predict wind turbine power output, Environ. Res. Lett., 8, 8 pp., doi: 10.1088/1748-9326/8/2/024009, 2013.

Clifton, A., and Lundquist, J.K.: Data clustering reveals climate impacts on local phenomena, J. Appl. Meteorol. Clim., 51, 1547–1557, doi:10.1175/JAMC-D-11-0227.1, 2012.

Clifton, A., Schreck, S., Scott, G., and Lundquist, J.K.,: Turbine inflow characterization at the National Wind Technology Center, J. Sol. Energ.-T ASME, 135, doi:10.1115/1.4024068, 2013.

Courtney, M., Wagner, R., and Lindelöw, P.: Testing and comparison of LIDARs for profile and turbulence measurements in wind energy, IOP Conference Series Earth and Environmental Science, 1, 1–14, doi:10.1088/1755-1307/1/1/012021, 2008.

Dörenkämper, M., Tambke, J., Steinfield, G., Heinemann, D., and Kühn, M.: Atmospheric impacts on power curves of multi-megawatt offshore wind turbines, Journal of Physics: Conference Series, 555, 1–11, doi: 10.1088/1742-6596/555/1/012029, 2014.

Elliott, D.L., and Cadogan, J.B.: Effects of wind shear and turbulence on wind turbine power curves, Proc. European Community Wind Energy Conference and Exhibition, Madrid, Spain, 1990.

GE Energy: 1.5 MW wind turbine, 2009, http://geosci.uchicago.edu/~moyer/GEOS24705/Readings/GEA14954C15-MW-Broch.pdf, last access: 21 January 2013.

Gottschall, J., and Peinke, J.: How to improve the estimation of power curves for wind turbines, Environ. Res. Lett., 3, 1–7, doi: 10.1088/1748-9326/3/1/015005, 2008.

Hunter, R., Pedersen, T.F., Dunbabin, P., Antoniou, I., Frandsen, S., Klug, H., Albers, A., and Lee, W.K.: European wind turbine testing procedure developments: Task 1: measurement method to verify wind turbine performance characteristics, Risø National Laboratory, Roskilde, Denmark,1–120, 2001.

IEC 61400-12-1 Ed 2.0: Wind turbines – Part 12-1: power performance measurements of electricity producing wind turbines, IEC, Geneva, Switzerland, 2015.

Kaiser, K., Hohlen, H., and Langreder, W.: Turbulence correction for power curves, Wind Energy Proc. European Wind Energy Conference and Exhibition, Madrid, 159–162, 2003.

Kelley, N.D.: Turbulence-turbine interaction: the basis for the development of the TurbSim Stochastic Simulator, NREL, Golden, Colo., 2011. http://www.nrel.gov/docs/fy12osti/52353.pdf, last access: 8 May 2016.

Lundquist, J.K., Churchfield, M.J., Lee, S., and Clifton, A.: Quantifying error of lidar and sodar Doppler beam swinging measurements of wind turbine wakes using computational fluid dynamics, Atmospheric Measurement Techniques, 8, 907–920, doi: 10.5194/amt-8-907-2015, 2015.

Mendoza, I., Hur, J., Thao, S., Curtis, A.: Power performance test report for the U.S. Department of Energy 1.5-megawatt wind turbine, NREL, Golden, Colo., 1–55, 2015, last access: 8 May 2016, http://www.nrel.gov/docs/fy15osti/63684.pdf.

Motta, M., Barthelmie, R.J., and Vølund, P.: The influence of non-logarithmic wind speed profiles on potential power output at Danish offshore sites, Wind Energy, 8, 219–236, 2005.

Muñoz-Esparza, D., Cañadillas, B., Neumann, T., and vanBeech, J.: Turbulent fluxes, stability and shear in the offshore environment: mesoscale modelling and field observations at FINO1, Journal of Renewable and Sustainable Energy, 4, 1–16, doi: 10.1063/1.4769201, 2012.

NWTC 135-m Tower Data: https://nwtc.nrel.gov/MetData, last access: 18 May 2016.

Pauliac, R.: WINDCUBE user's manual, 2009.

Poulos, G.S., Bossert, J.E., Pielke, R.A., and McKee, T.B.: The interaction of katabatic flow and mountain waves I: observations and idealized simulations, J. Atmos. Sci., 57, 1919–1936, 2000.

Poulos, G.S., Bossert, J.E., Pielke, R.A., and McKee, T.B.: The interaction of katabatic flow and mountain waves II: case study analysis and conceptual model, J. Atmos. Sci., 64, 1857–1879, 2007.

Rareshide, E., Tindal, A., Johnson, C., Graves, A.M., Simpson, E., Bleeg, J., Harris, T., and Schoborg, D.: Effects of complex wind regimes on turbine performance, AWEA Windpower 2009 meeting, Chicago, Ill., 2009.

Rhodes, M.E., and Lundquist, J.K.: The effect of wind-turbine wakes on summertime US Midwest atmospheric wind profiles as observed with ground-based Doppler LIDAR, Boundary-Layer Meteorol. 149, 85–103, doi:10.1007/s10546-013-9834-x, 2013.

Rinker, J.M., Gavin, H.P., Clifton, A., Veers, P.S., and Kilcher, L.F.: Temporal coherence: a model for non-stationarity in natural and simulated wind records, Boundary-Layer Meteorol., 159, 373–389, doi: 10.1007/s10546-015-0121-x, 2016.

Stull, R.B.: An Introduction to Boundary Layer Meteorology, Kluwer Academic Publishers, Netherlands, 1988.

Sumner, J., and Masson, C.: Influence of atmospheric stability on wind turbine power performance curves, J. Sol. Energ.-T ASME, 128, 531–538, doi:10.1115/1.2347714, 2006.

van den Berg, G.P.: Wind turbine power and sound in relation to atmospheric stability, Wind Energy, 11, 151–169, 2008.

Vanderwende, B., and Lundquist, J.K.: The modification of wind turbine performance by statistically distinct atmospheric regimes, Environ. Res. Lett., 7, 1–7, doi:10.1088/1748-9326/7/3/034035, 2012.

Wagenaar, J.W., and Eecen, P.J.: Dependence of power performance on atmospheric conditions and possible corrections, European Wind Energy Association (EWEA) 2011 conference, Brussels, Belgium, 2011. http://www.ecn.nl/docs/library/report/2011/m11033.pdf, last access: 9 May 2016.

Wagner, R., Antoniou, I., Pedersen, S., Courtney, M., and Jorgensen, H.: The influence of the wind speed profile on wind turbine performance measurements, Wind Energy, 12, 348–362, doi:10.1002/we.297, 2009.

Walton, R.A., Takle, E.S., and Gallus Jr., W.A.: Characteristics of 50–200-m winds and temperatures derived from an Iowa tall-tower network, J. Appl. Meteorol. Clim., 53, 2387–2393, doi:10.1175/JAMC-D-13-0340.1, 2014.

Wharton, S., and Lundquist, J.K.: Atmospheric stability affects wind turbine power collection, Environ. Res. Lett., 7, 1–9, doi:10.1088/1748-9326/7/014005, 2012a.

Wharton, S. and Lundquist, J.K.: Assessing atmospheric stability and its impacts on rotor-disk wind characteristics at an onshore wind farm, Wind Energy, 15, 525–546, doi:10.1002/we.483, 2012b.

Wind Energ. Sci. Discuss., doi:10.5194/wes-2016-21, 2016
Manuscript under review for journal Wind Energ. Sci.
Published: 17 June 2016

eawe european academy of wind energy
Open Access WIND ENERGY SCIENCE DISCUSSIONS

Table 1. 135m met tower instrument information

Type	Instrument	Mounting Heights (m)	Accuracy
Cup anemometer	Met One SS-201	3, 10, 38, 87, 122	0.5 m s^{-1}
Cup anemometer	Thies 4.3351.10.0000	30, 55, 80, 105, 130	0.2 m s^{-1}
Wind vane	Met One SD-201	3, 10, 38, 87, 122	3.6°
Air temperature sensor	Met One T-200A platinum RTD	3, 38, 87	0.1°C
Differential temperature sensor	Met One T-200A	38, 87, 122	0.1°C
Sonic anemometer	ATI 'K' type	15, 41, 61, 74, 100, 119	0.01 m s^{-1}
Boom triaxial acceleration sensor	Summit 34201A	15, 41, 61, 74, 100, 119	
Sonic temperature	ATI 'K' type	15, 41, 61, 74, 100, 119	0.1°C
Barometric pressure sensor	AIR AB-2AX	3	
Dewpoint temperature sensor	Therm-x 9400ASTD	3, 38, 87, 122	
Precipitation sensor	Vaisala DRD11A	3	

Wind Energ. Sci. Discuss., doi:10.5194/wes-2016-21, 2016
Manuscript under review for journal Wind Energ. Sci.
Published: 17 June 2016

eawe european academy of wind energy
Open Access WIND ENERGY SCIENCE DISCUSSIONS

Table 2. Defined stability regimes

Stability class	R_B	L (m)	α
Unstable conditions	$R_B < -0.03$	$-1{,}000 < L \leq 0$	$\alpha < 0.11$
Neutral conditions	$-0.03 < R_B < 0.03$	$\lvert L \rvert \geq 1{,}000$	$0.11 < \alpha < 0.17$
Stable conditions	$R_B > 0.03$	$0 \leq L < 1{,}000$	$\alpha > 0.17$

Table 3. Defined turbulence regimes

Turbulence regime	**TI (%)**	**TKE ($m^2 s^{-2}$)**
High turbulence	TI > 20	TKE > 5
Medium turbulence	15 < TI < 20	2.5 < TKE < 5
Low turbulence	TI < 15	TKE < 2.5

Table 4. AEP in megawatt-hours/year calculated for different atmospheric and turbulence regimes using a Weibull distribution with a scale factor of 10.13 m s^{-1} and a shape factor of 2.62.

	No filter	**TI filter**	**α filter**	**R_B filter**
AEP (MWh/y)	7,546.5	7,384.1	7,343.9	6,780.2

Table 5. AEP in percentage calculated for different filter regimes using a Weibull distribution with a scale factor of 10.13 m s^{-1} and a shape factor of 2.62. Medium regime is set at 100 % and low and high regimes are percentages compared to the medium regime. Boxes with the highest value within that row are italicized.

Filter	**Low regime**	**Medium regime**	**High regime**
TI	88.11	*100.00*	84.63
α	101.18	100.00	*102.20*
R_B	*147.80*	100.00	118.89

Wind Energ. Sci. Discuss., doi:10.5194/wes-2016-21, 2016
Manuscript under review for journal Wind Energ. Sci.
Published: 17 June 2016

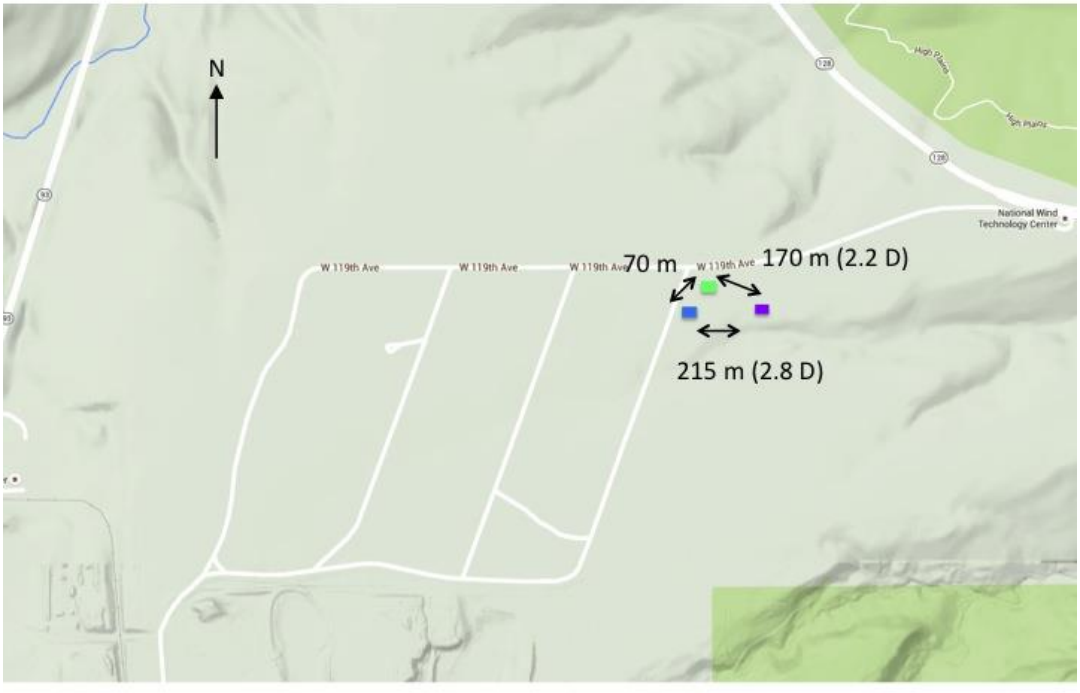

Figure 1. Top: Google Maps image of the NWTC with instrument locations. The green rectangle represents the location of the met tower, the purple rectangle represents the location of the turbine, and the blue rectangle represents the location of the lidar. Map Data © 2016 Google.

Wind Energ. Sci. Discuss., doi:10.5194/wes-2016-21, 2016
Manuscript under review for journal Wind Energ. Sci.
Published: 17 June 2016

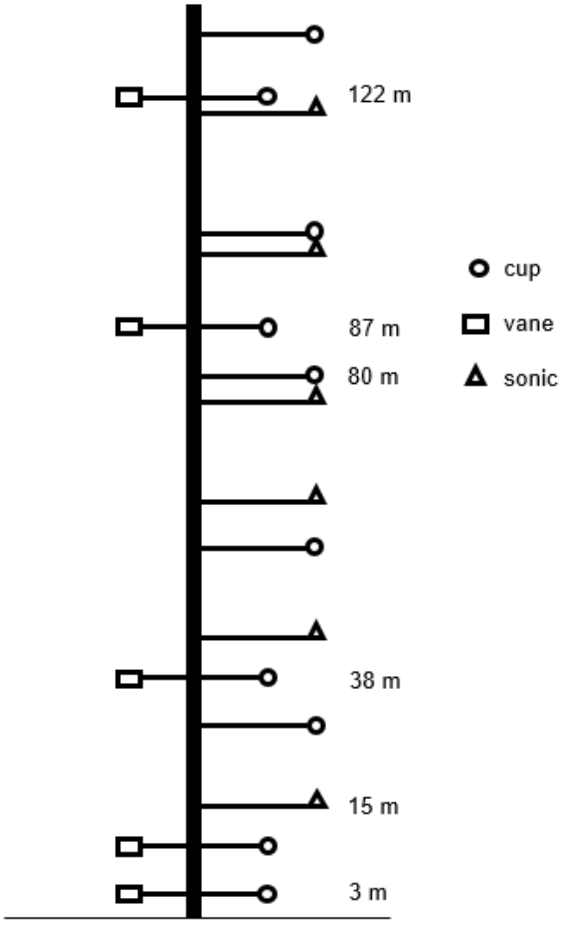

Figure 2. 135m meteorological tower configuration. A few key heights are labeled. This tower is slightly different from the M4 tower described in Clifton et al. (2013), but data are available online (NWTC, 2016).

Wind Energ. Sci. Discuss., doi:10.5194/wes-2016-21, 2016
Manuscript under review for journal Wind Energ. Sci.
Published: 17 June 2016

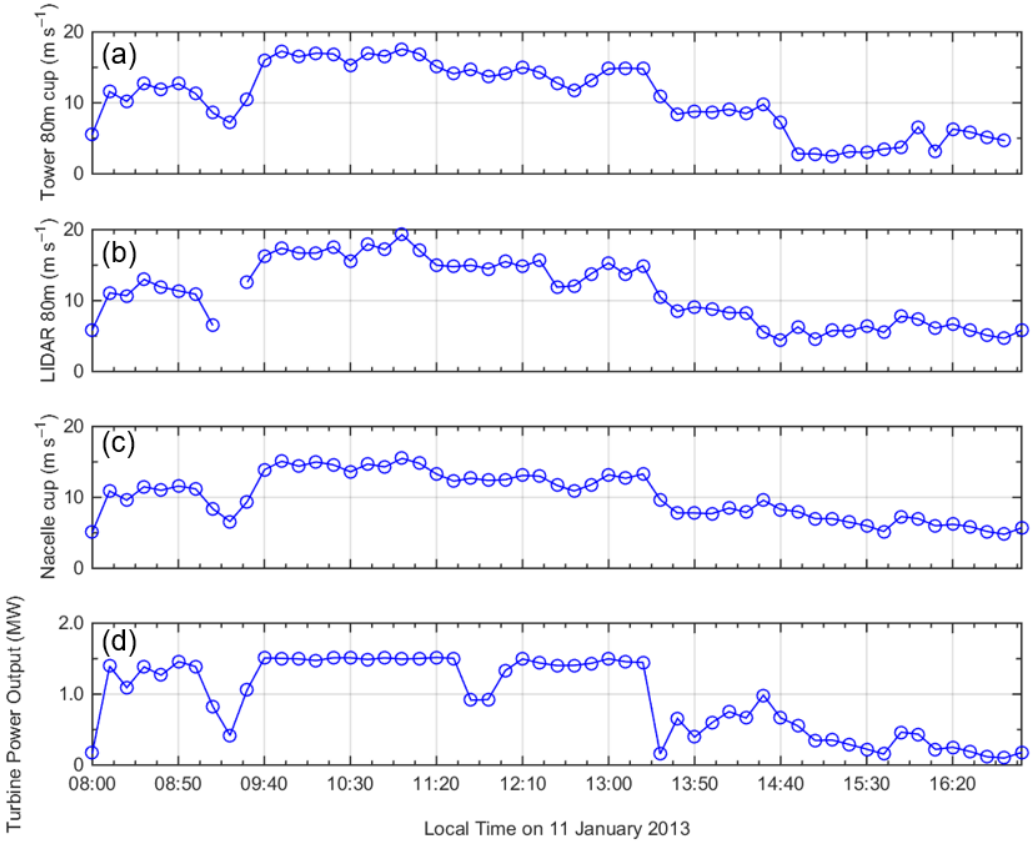

Figure 3. Time series from 11 January 2013 from 08:00 to 17:00 Mountain Standard Time (MST): (a) is a time series of 80m wind speeds measured by the cup on the tower; (b) is a time series of 80m wind speeds measured by the lidar; (c) is a time series of the hub height wind speeds measured by the cup anemometer on the nacelle; and (d) is a time series of the power output from the turbine.

Wind Energ. Sci. Discuss., doi:10.5194/wes-2016-21, 2016
Manuscript under review for journal Wind Energ. Sci.
Published: 17 June 2016

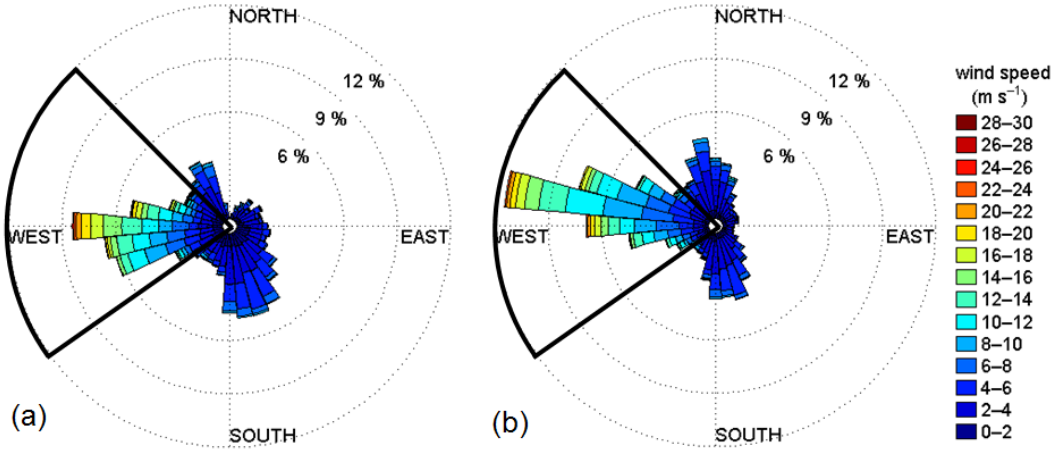

Figure 4. Wind roses for (a) lidar 80 m and (b) met tower 87 m (altitude closest to hub height with both a cup and vane). Wind bins are 2 m s^{-1} and wind directions bins are 10°. Black outline highlights the chosen wind direction sector.

Wind Energ. Sci. Discuss., doi:10.5194/wes-2016-21, 2016
Manuscript under review for journal Wind Energ. Sci.
Published: 17 June 2016

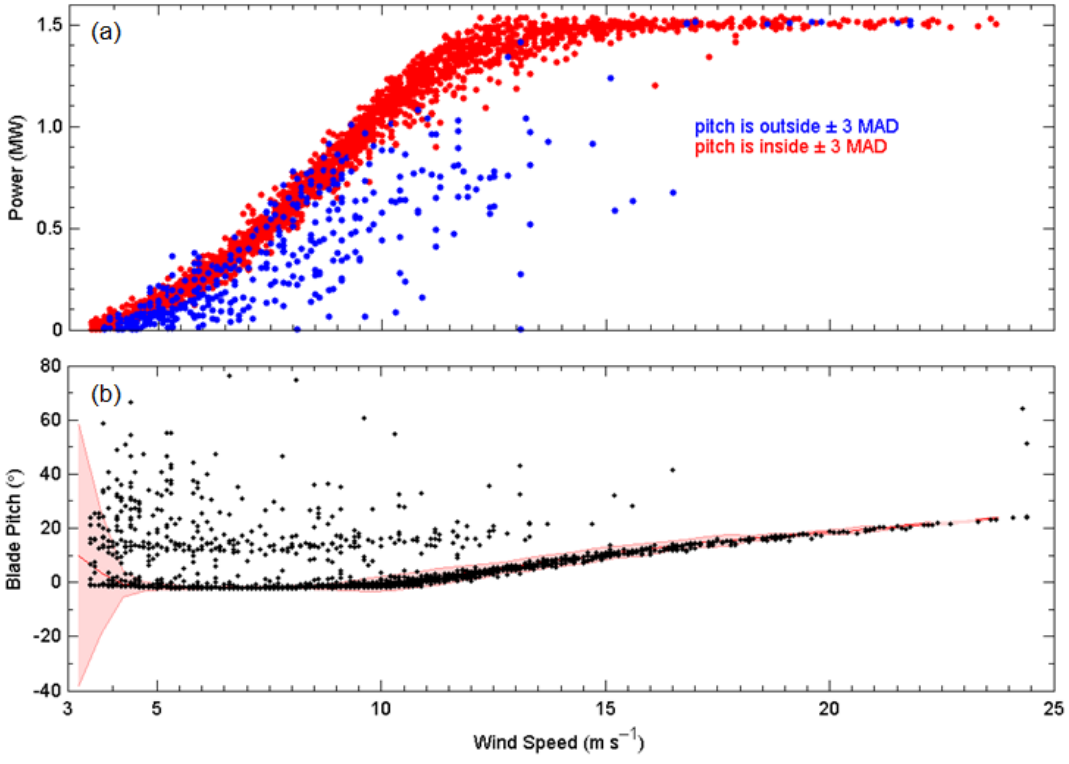

Figure 5. (a) Scatter power curve using the tower 80m wind speed. The blue scatter shows the points that are outside of the MAD envelope in (b) and the red scatter shows the points that are within the MAD envelope in (b); (b) blade pitch angle from a single blade versus tower 80m wind speed. Red envelope represents ± 3 MAD of the blade pitch angle within wind speed bins 0.5 m s^{-1} wide.

Wind Energ. Sci. Discuss., doi:10.5194/wes-2016-21, 2016
Manuscript under review for journal Wind Energ. Sci.
Published: 17 June 2016

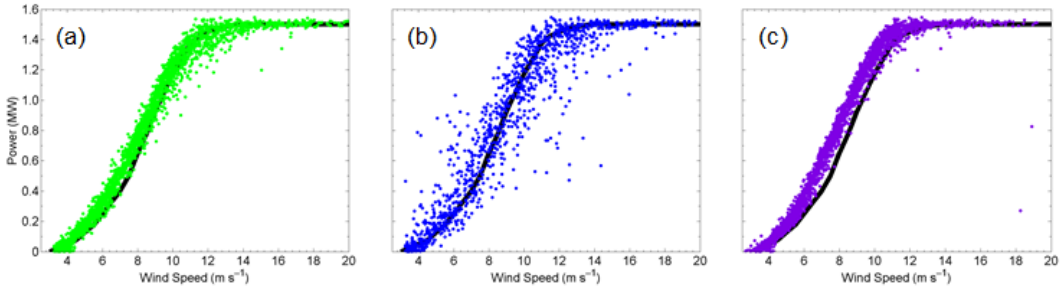

Figure 6. Power curves after filtering for wind speeds between 3.5 and 25 m s^{-1}, wind directions between 235°and 315°, and blade pitch angle within ± 3 MAD: (a) turbine power production versus 80m cup anemometer wind speed from the met tower; (b) turbine power production versus 80m wind speed from the lidar; (c) turbine power production versus hub height wind speed from the anemometer on the nacelle. Grey line represents an approximation of the manufacturer power curve for the GE 1.5sle (GE Energy, 2009). Wind speed is normalized for density following IEC 61400-12-1 (2015).

Wind Energ. Sci. Discuss., doi:10.5194/wes-2016-21, 2016
Manuscript under review for journal Wind Energ. Sci.
Published: 17 June 2016

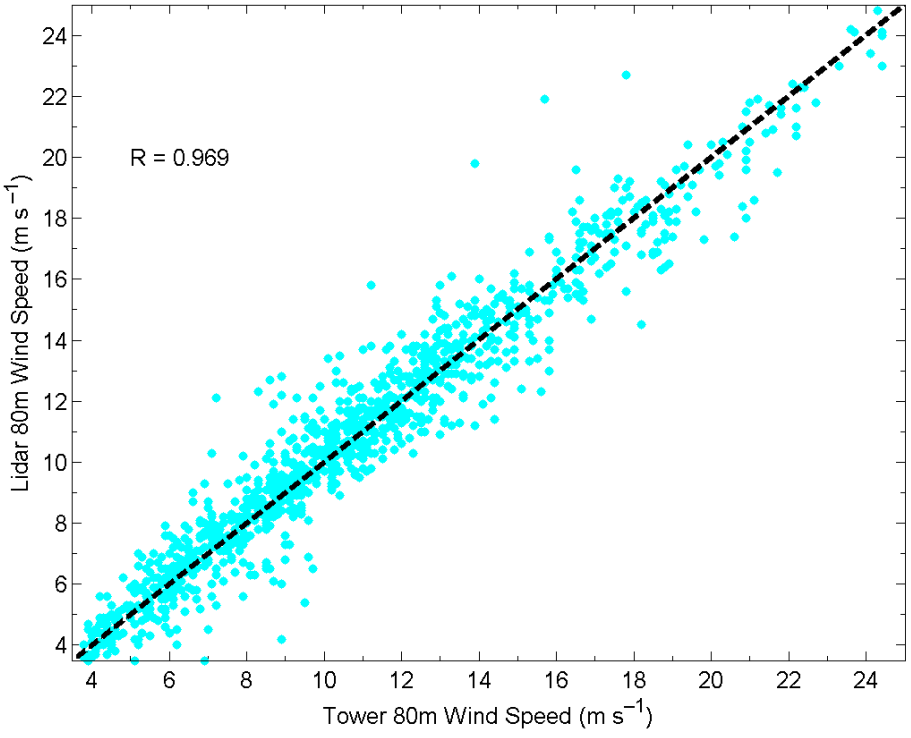

Figure 7. Lidar 80m wind speeds compared to tower 80m wind speeds filtered for wind speeds between 3.5 and 25.0 m s^{-1}, wind directions between 235° and 315°, and blade pitch angle within ± 3 MAD. Black dashed line represents a 1:1 relationship.

Wind Energ. Sci. Discuss., doi:10.5194/wes-2016-21, 2016
Manuscript under review for journal Wind Energ. Sci.
Published: 17 June 2016

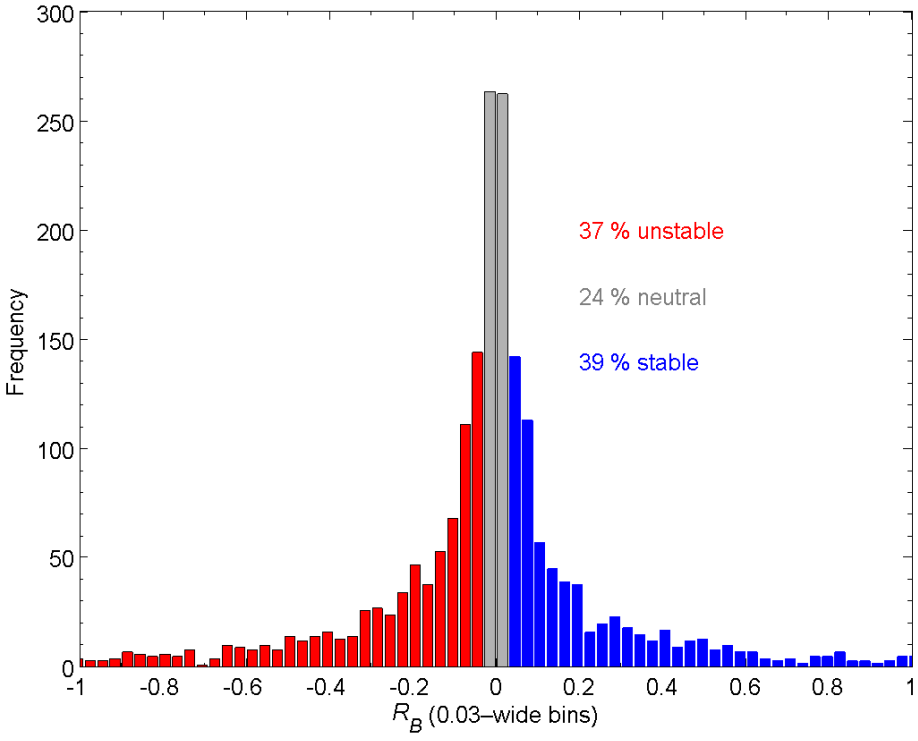

Figure 8. R_B distribution using thresholds in Table 2. Includes data filtered for tower 80m wind speeds between 3.5 and 25.0 m s^{-1}, 87m wind directions between 235° and 315°, and blade pitch angle within ± 3 MAD.

Wind Energ. Sci. Discuss., doi:10.5194/wes-2016-21, 2016
Manuscript under review for journal Wind Energ. Sci.
Published: 17 June 2016

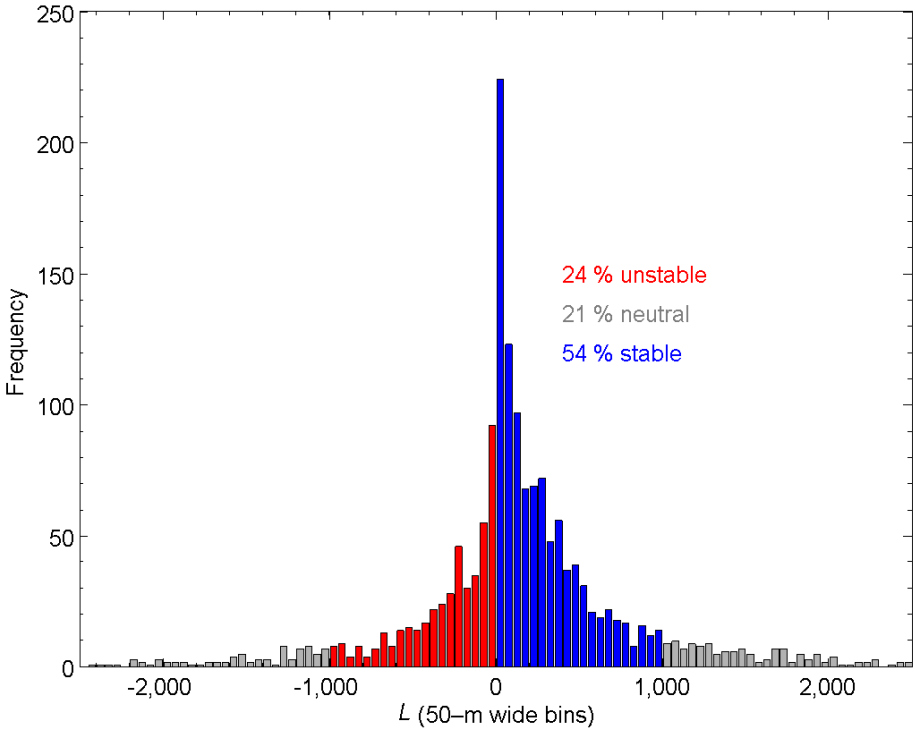

Figure 9. *L* distribution using thresholds in Table 2. Note that some neutral cases are outside of these axes. Includes data filtered for tower 80m wind speeds between 3.5 and 25.0 m s^{-1}, 87m wind directions between 235° and 315°, and blade pitch angle within ± 3 MAD.

Wind Energ. Sci. Discuss., doi:10.5194/wes-2016-21, 2016
Manuscript under review for journal Wind Energ. Sci.
Published: 17 June 2016

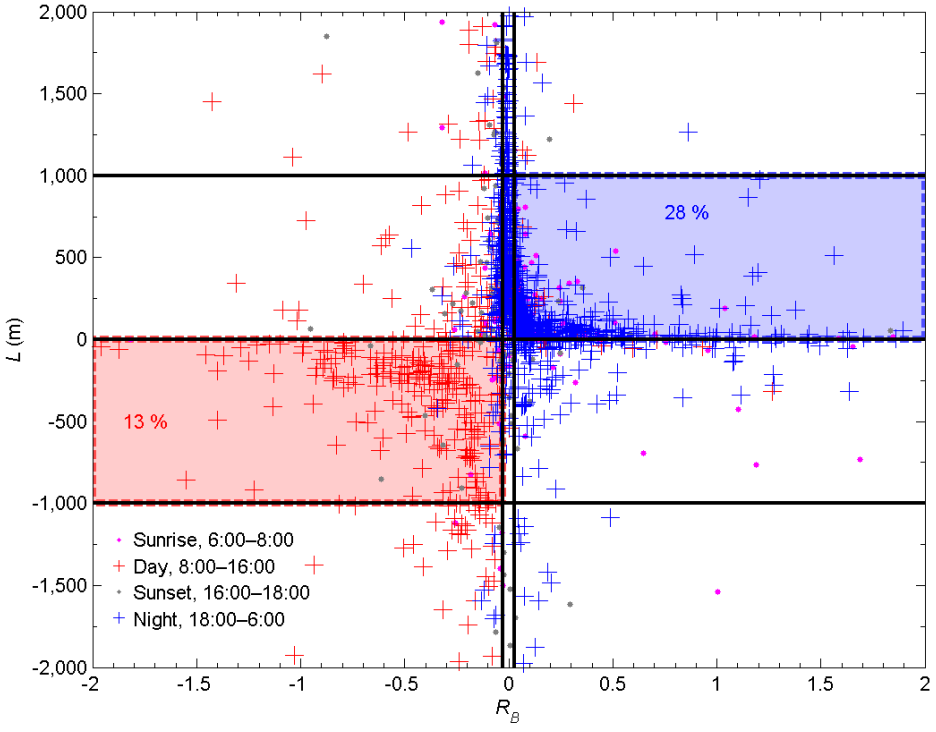

Figure 10. L versus R_B. Blue box represents where both L and R_B agree on the stable conditions; percentage represents the percentage of data points in this box. Red box represents where both L and R_B agree on the unstable conditions; percentage represents the percentage of data points in this box. Includes data filtered for tower 80m wind speeds between 3.5 and 25 m s^{-1}, 87m wind directions between 235° and 315°, and blade pitch angle within $\pm$ 3 MAD.

Wind Energ. Sci. Discuss., doi:10.5194/wes-2016-21, 2016
Manuscript under review for journal Wind Energ. Sci.
Published: 17 June 2016

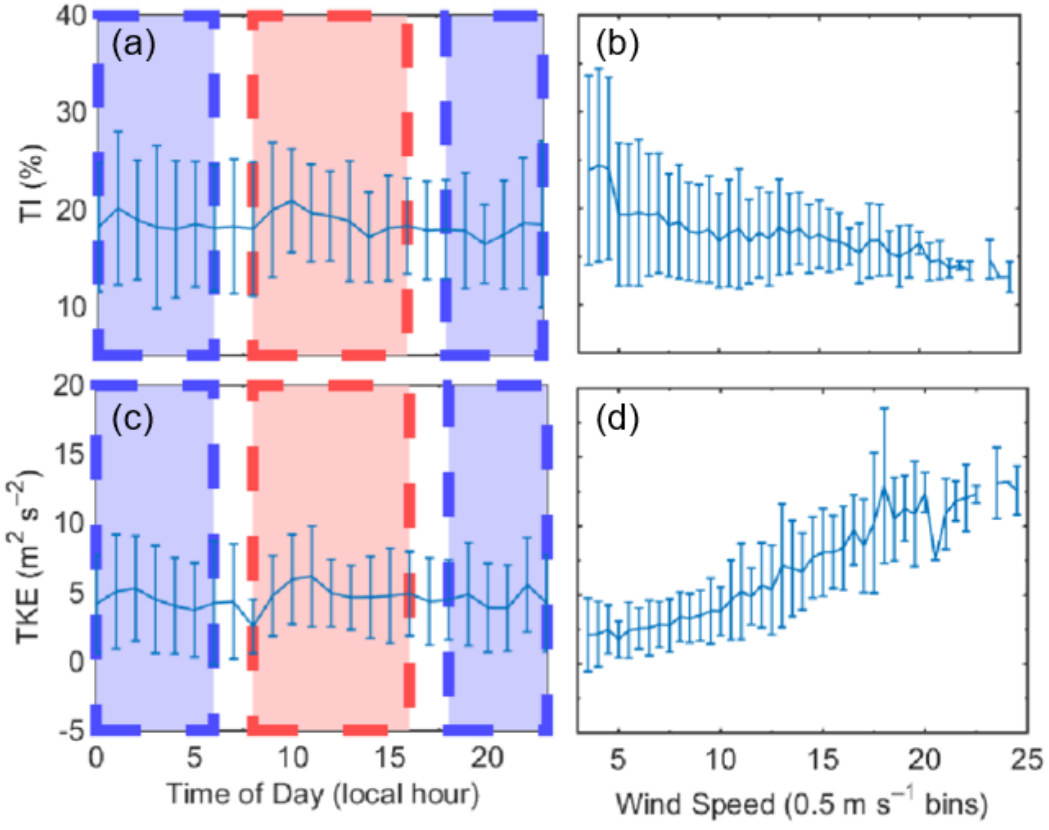

Figure 11. TI (a) and TKE (c) calculated with near hub height tower measurements versus time of day, where hour 0 and hour 24 represent midnight. The blue line represents the mean TI in the corresponding hour and the error bar represents the standard deviation. The blue rectangle represents nighttime hours and the red rectangle represents daytime hours. Mean and standard deviation of TI (b) and TKE (d) calculated with near hub height tower measurements in each wind speed bin. Includes data filtered for tower 80m wind speeds between 3.5 and 25.0 m s^{-1}, 87m wind directions between 235° and 315°, and blade pitch angle within ± 3 MAD.

Wind Energ. Sci. Discuss., doi:10.5194/wes-2016-21, 2016
Manuscript under review for journal Wind Energ. Sci.
Published: 17 June 2016

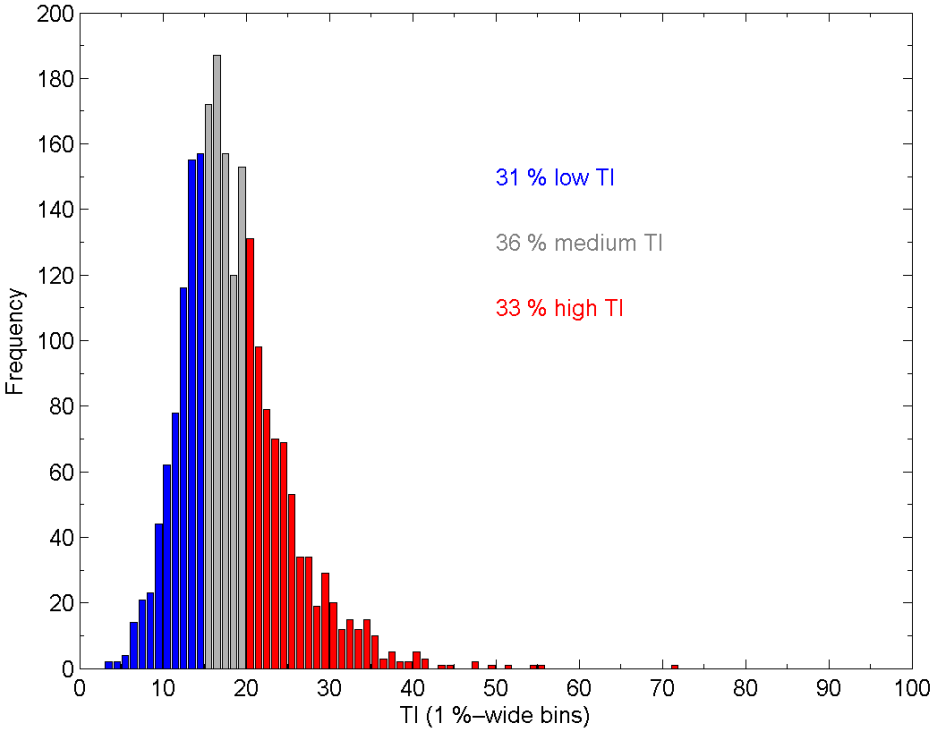

Figure 12. TI distribution using thresholds in Table 3. Includes data filtered for tower 80m wind speeds between 3.5 and 25 m s^{-1}, 87m wind directions between 235° and 315°, and blade pitch angle within $\pm$ 3 MAD.

Wind Energ. Sci. Discuss., doi:10.5194/wes-2016-21, 2016
Manuscript under review for journal Wind Energ. Sci.
Published: 17 June 2016

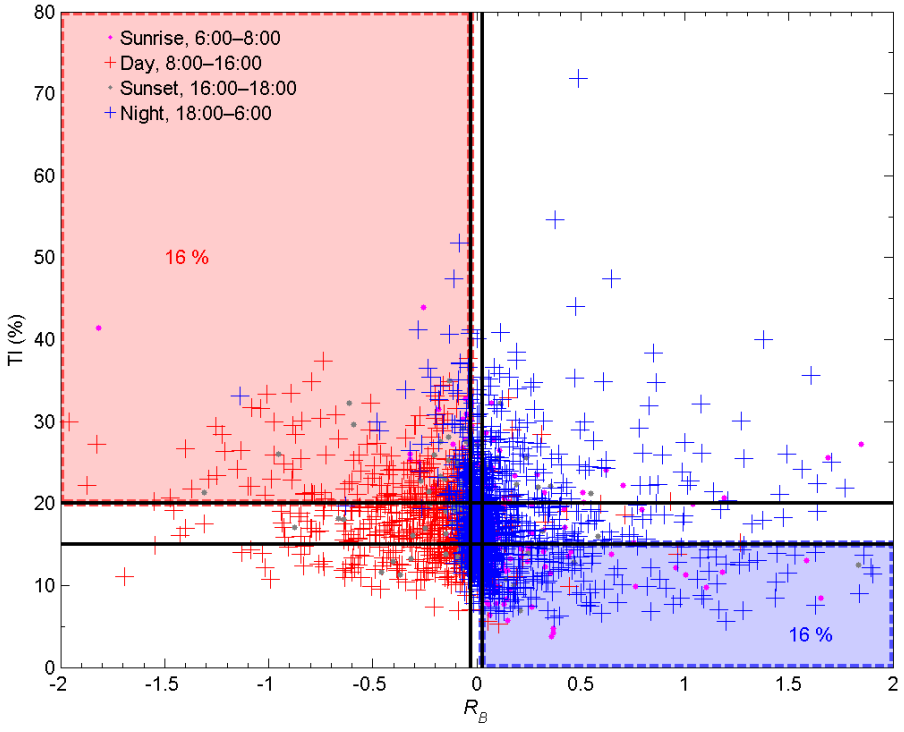

Figure 13. TI versus R_B . Blue box represents where both TI and R_B agree on the stable conditions; percentage represents the percentage of data points in this box. Red box represents where both TI and R_B agree on the unstable conditions; percentage represents the percentage of data points in this box. Includes data filtered for tower 80m wind speeds between 3.5 and 25 m s^{-1}, 87m wind directions between 235° and 315°, and blade pitch angle within $\pm$ 3 MAD.

Wind Energ. Sci. Discuss., doi:10.5194/wes-2016-21, 2016
Manuscript under review for journal Wind Energ. Sci.
Published: 17 June 2016

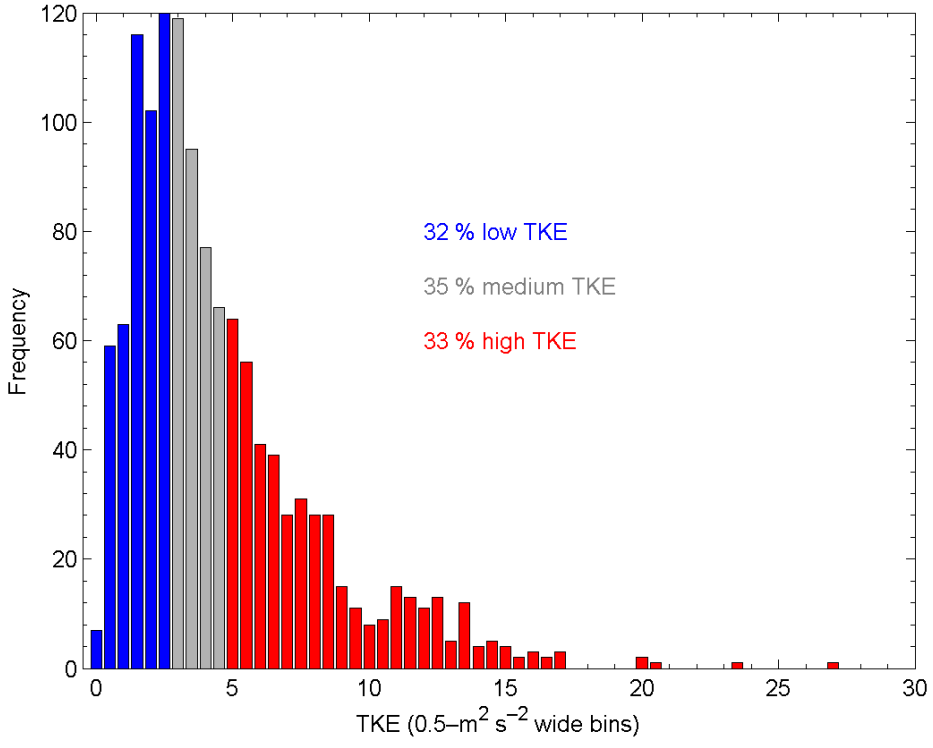

Figure 14. TKE distribution using thresholds in Table 3. Includes data filtered for tower 80m wind speeds between 3.5 and 25.0 m s^{-1}, 87m wind directions between 235° and 315°, and blade pitch angle within ± 3 MAD.

Wind Energ. Sci. Discuss., doi:10.5194/wes-2016-21, 2016
Manuscript under review for journal Wind Energ. Sci.
Published: 17 June 2016

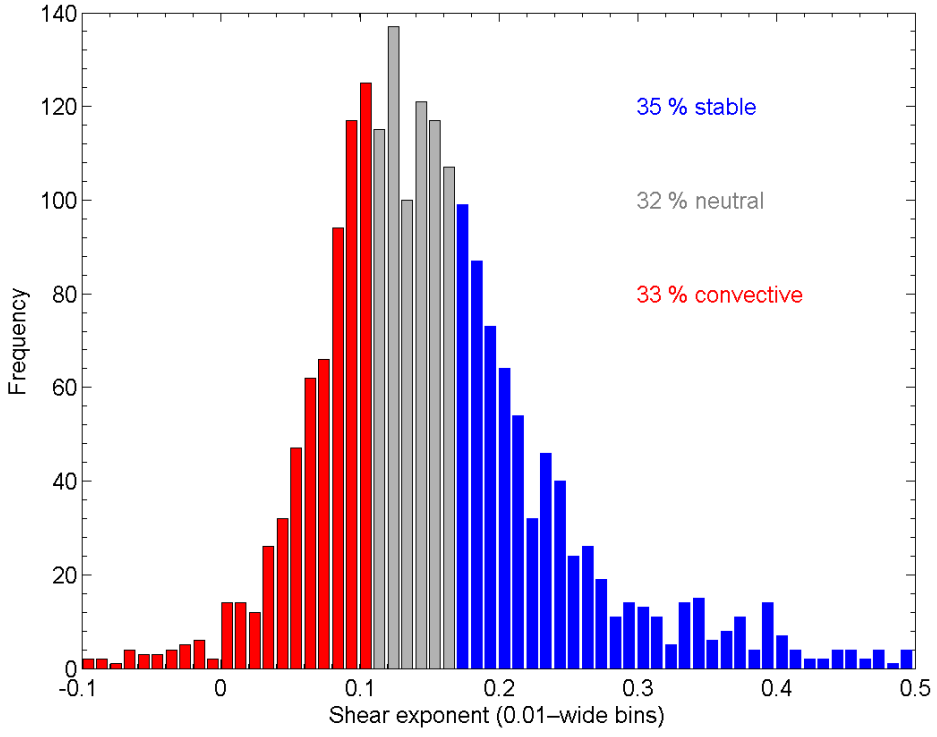

Figure 15. Shear exponent distribution using thresholds in Table 2. Includes data filtered for tower 80m wind speeds between 3.5 and 25.0 m s^{-1}, 87m wind directions between 235° and 315°, and blade pitch angle within ± 3 MAD.

Wind Energ. Sci. Discuss., doi:10.5194/wes-2016-21, 2016
Manuscript under review for journal Wind Energ. Sci.
Published: 17 June 2016

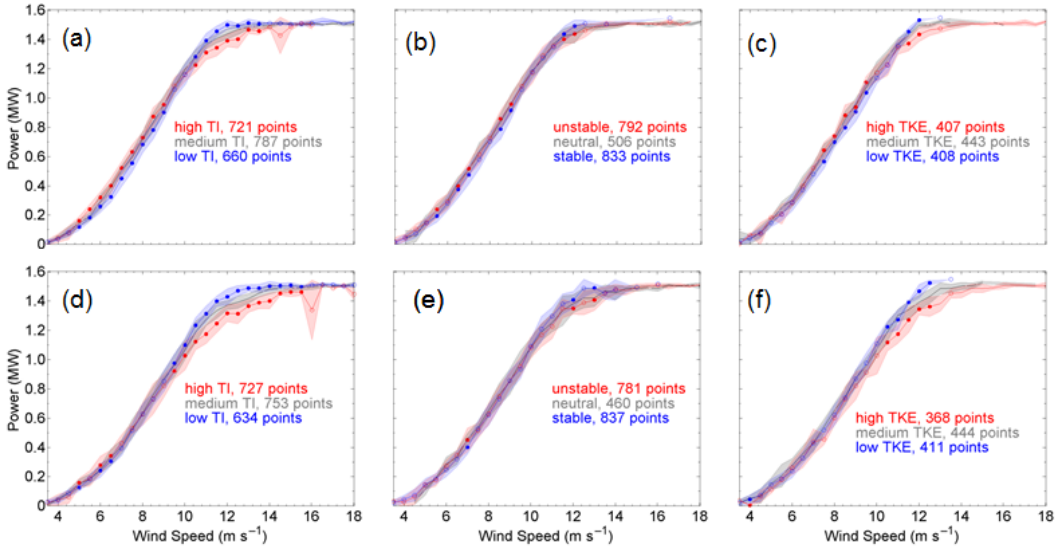

Figure 16. Nacelle anemometer power curves with (a) TI regimes; (b) R_B regimes; and (c) TKE regimes. Eighty-meter tower anemometer power curves with (d) TI regimes; (e) R_B regimes; and (f) TKE regimes. Statistically distinct differences within each wind speed bin between the regimes are determined by the Wilcoxon rank sum test with a 1 % significance level and denoted by closed circles. Includes data filtered for tower 80m wind speeds between 3.5 and 25.0 m s^{-1}, 87m wind directions between 235° and 315°, and blade pitch angle within $\pm$ 3 MAD. Envelopes represent ± 1 MAD for each wind speed bin.

Wind Energ. Sci. Discuss., doi:10.5194/wes-2016-21, 2016
Manuscript under review for journal Wind Energ. Sci.
Published: 17 June 2016

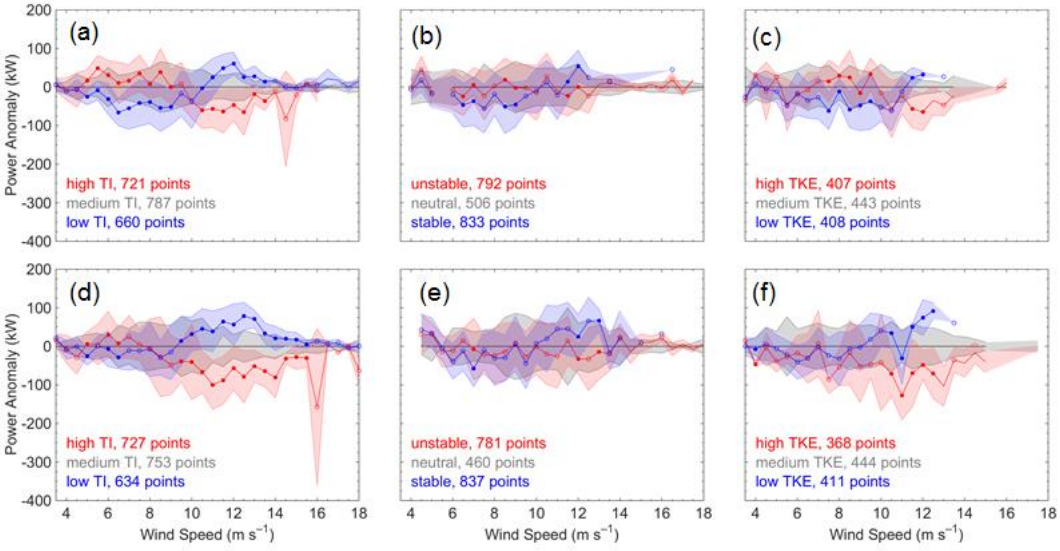

Figure 17. Nacelle anemometer power curves shown as the anomaly from the neutral or medium power curve of the (a) TI regimes; (b) R_B regimes; and (c) TKE regimes. Eighty-meter tower anemometer power curves shown as the anomaly from the neutral or medium power curve of the (d) TI regimes; (e) R_B regimes; and (f) TKE regimes. Statistically distinct differences within each wind speed bin between the regimes are determined by the Wilcoxon rank sum test with a 1 % significance level and denoted by closed circles. Includes data filtered for tower 80m wind speeds between 3.5 and 25.0 m s^{-1}, 87m wind directions between 235° and 315°, and blade pitch angle within ± 3 MAD. Envelopes represent ± 1 MAD for each wind speed bin.